Novel cast-aged MnCuNiFeZnAl alloy with good damping capacity and high usage temperature towards engineering application

Wenbo Liu,[a,b] Ning Li,[a,*] Zhenyu Zhong,[a] Jiazhen Yan,[a] Dong Li,[a] Ying Liu,[c] Xiuchen Zhao,[c] and Sanqiang Shi[b]

[a] School of Manufacturing Science and Engineering, Sichuan University, Chengdu, 610065, P. R. China

[b] Department of Mechanical Engineering, The Hong Kong Polytechnic University, Hung Hom, Kowloon, Hong Kong

[c] School of Materials Science and Engineering, Beijing Institute of Technology, Beijing 100081, PR China

Tel: +86-028-85405320; Fax: +86-028-85403408; E-mail: liuwenbo_8338@163.com.

Abstract

Novel cast-aged Mn-26.0Cu-2.0Ni-2.0Fe-2.0Zn-3.0Al (wt.%) alloy with good damping capacity and high usage temperature has been well designed and developed in this work, which can act as a promising candidate toward engineering applications. The microstructure, damping capacity and usage temperature were investigated systematically by X-ray diffraction, optical microscopy, scanning electron microscopy, energy dispersive spectroscopy, and dynamic mechanical analyzer. The results show that heat treatment has a significant influence on the damping capacity and usage temperature of as-cast MnCuNiFeZnAl alloy. Compared to the original as-cast alloy with internal friction (Q^{-1}) of 3.0×10^{-2} at a strain amplitude $\varepsilon=2\times10^{-4}$ and usage temperature of 43℃, the largest Q^{-1} (5.0×10^{-2}) and highest usage temperature (70℃) can be obtained simultaneously by ageing treatment at 435℃ for 2h, while homogenization-ageing, solution-ageing and overageing can just result in the limited improvement of damping capacity and usage temperature. This is because the highest nanoscale Mn segregation in Mn dendrites can be formed by spinodal decomposition during ageing, while carrying out the homogenization or solution treatment prior to the ageing, as well as overageing treatment can cause the weakening of Mn segregation at the macro/nano-scale and even the precipitation of α-Mn, thus leading to the undesirable damping capacity and usage temperature.

Keywords: Mn-Cu based damping alloys; Casting; Internal friction; Usage temperature; Heat treatment; Phase transformation

1. Introduction

Manganese-copper based alloys have been extensively studied because of their excellent damping capacity and versatile magnetic features [1,2]. The high damping capacity can be mainly attributed to magnetic domain boundaries and lattice distortion induced {110} twin boundaries [3,4], evidently different from other types of damping alloys, such as Ni-Ti based, Fe-Ga based and Mg-Zn based alloys [5-8]. The {110} twinning structure normally forms during face centered cubic to face centered tetragonal (f.c.c-f.c.t) phase transformation below phase transformation point (T_t) of alloy. It has been found that the formation of twinning structure and introduction of twinning dislocations can effectively reduce the strain energy caused by f.c.c-f.c.t phase transformation below T_t, as well as the T_t is directly dependent on the Mn content in Mn-Cu based alloys [9,10]. Typically, the high damping capacity can be readily obtained in quenched Mn-Cu based alloys with more than 82 at.% Mn. However, the high Mn content in alloy matrix is fatally detrimental to its workability, which will go against their engineering applications. It has been reported that Mn-Cu based alloys with relatively low Mn content also could obtain the high T_t and good damping capacity through ageing treatment in a proper temperature range [11]. Typically, as ageing in the temperature range of miscibility gap, the γ parent phase in Mn-Cu based alloys spinodally decomposed into nanoscale Mn-rich regions and nanoscale Cu-rich regions, characterized as the ‘tweed’ microstructure [12-14], which is considerably beneficial to the improvement of damping capacity. Obviously, this is an effective approach to achieve both superior damping capacity and good

workability.

Forged M2052 (Mn-20Cu-5Ni-2Fe, at.%) alloy, a typical Mn-Cu based high-damping material with low Mn content developed by Kawahara et al. [15], had been widely studied in the past decades. Compared to the forging technique, one-step molding casting has thus far received considerable recognition for the distinct advantages of simple manufacturing process, low integrated cost and high production efficiency. For example, the influence factors (resonant frequency, strain amplitude, cooling rate, holding temperature/time, etc.), microstructure and damping mechanism of as-cast M2052 alloy with good damping capacity has been investigated in our previous work and the literature [16-21]. Nevertheless, we found that the M2052 alloy was defective in castability. Thus, in order to further solve this issue, we consider that both Zn and Al elements could be designed to add in the alloy matrix; meanwhile, the optimal heat treatment process for both good damping capacity and high usage temperature of the developed as-cast alloy needs to be screened out in light of their equal significance toward engineering applications.

In this report, a novel Mn-26.0Cu-2.0Ni-2.0Fe-2.0Zn-3.0Al (wt.%) alloy has been prepared to systematically investigate the heat treatment process dependency of its damping capacity and usage temperature. The results show that heat treatment process has a crucial influence on the damping capacity and usage temperature of the as-cast MnCuNiFeZnAl alloy. Among seven types of designed heat treatment processes, the largest Q^{-1} and highest usage temperature can be obtained simultaneously by direct ageing at 435℃ for 2h, indicative of a promising candidate toward engineering

applications. Based on our understanding of damping machanism of as-cast Mn-Cu based alloys, the probably reasons are discussed in detail accordingly.

2. Experimental procedure

Mn-26.0Cu-2.0Ni-2.0Fe-2.0Zn-3.0Al (wt.%) alloy ingots was prepared by vacuum induction melting with pure metals in an inert argon atmosphere. The molten alloy was cast into the salica-sand mold through a sprue to get slow cooling rate, and then the sprue of ingots was cut out. Chemical composition of the as-prepared alloy was determined to be Mn-22.68Cu-1.89Ni-1.99Fe-1.70Zn-6.16Al (at.%).

The specimens from the alloy ingots were subjected to different heat treatments and then divided into seven types assigned to 1#-7#, respectively. Table 1 shows the detailed heat treatment conditions for each type of specimen, in which specimen 1# is the original as-cast MnCuNiFeZnAl alloy without subsequent heat treatment as a reference. The main aims to design these heat treatment conditions are as follows: Homogenization treatment can be used for reducing dendritic segregation, solution treatment for impurities immobilization, as well as different ageing times for finding out the optimal parameters for excellent damping capacity and usage temperature.

For metallographic observation, all specimens were etched in a mixed solution of 10 g $FeCl_3.H_2O$, 30 ml HCl (37.5 wt.%) and 120 ml CH_3OH after mechanical polishing. Dendrite microstructure and composition distribution of specimens were characterized and analyzed using scanning electron microscopy (SEM, TESCAN VEGA II) equipped with energy dispersive spectroscopy (EDS). The phase structure and lattice parameter of specimens were identified by X-ray diffraction (XRD,

Panalytical X'pert Pro X-Ray diffractometer, operated at 40 kV and 40 mA) with Cu Kα radiation, and all the diffraction profiles were obtained in continuous modes at a scan speed of 2 °/min. The specimens for XRD measurement, in sizes of 10×10×1 mm^3, were carefully prepared to remove surface strain.

Dynamic Mechanical Analysis (DMA, Q800 TA) was used for damping capacity measurement of specimens. Each specimen under dual-cantilever mode possessed a dimension of 0.8×10×35 mm^3, and the resonant frequency and testing temperature were 1 Hz and 25℃, respectively. When the applied strain amplitude at the specimen surface varying from 0 to 2.5×10^{-4}, the damping capacity of the experimental alloy is characterized by internal friction Q^{-1} ($Q^{-1}=\tan\delta$, as described detailedly in the Ref. [22]). For the measurements of temperature dependent damping capacities, the test conditions were as follows: the strain amplitude (ε) was 2.0×10^{-4}, the vibration frequency 1 Hz, the temperature range from room temperature (25℃) to 120℃, and the heating rate was 2 ℃/min.

3. Results and discussion

The strain sweeping of DMA is first used to obtain the damping capacity curves of the as-cast MnCuNiFeZnAl alloys under different heat treatment conditions at a test frequency of 1 Hz. Fig. 1 shows the strain-amplitude dependence of Q^{-1} of as-cast MnCuNiFeZnAl alloys subjected to different heat treatments containing ageing for 4h, corresponding to specimens 1#-4# respectively. As can be seen clearly, the Q^{-1} of all the four specimens exhibits an evident positive correlation with the increase of strain amplitude, implying the strain-amplitude-dependent damping capacity. At the typical

strain-amplitude of $\varepsilon=2\times10^{-4}$, the Q^{-1} is 3.0×10^{-2}, 4.7×10^{-2}, 4.9×10^{-2} and 3.9×10^{-2} for specimens 1#-4#, respectively. It indicates that the original as-cast MnCuNiFeZnAl alloy has certain damping capacity, which can be further improved by subsequently carrying out homogenization-ageing, solution-ageing and ageing for 4h respectively, in which the solution-ageing for 4h can result in the highest damping capacity among them.

For comparison, Fig. 2 shows the strain-amplitude dependence of Q^{-1} of as-cast MnCuNiFeZnAl alloys subjected to similar heat treatments containing ageing for 2h, corresponding to specimens 1#, 5#-7# respectively. Obviously, there is quite distinct difference between results in Fig. 1 and Fig. 2 except for the similar change tendency of strain-amplitude-dependent damping capacity. At $\varepsilon=2\times10^{-4}$, the Q^{-1} is 3.0×10^{-2}, 4.5×10^{-2} ,4.7×10^{-2} and 5.0×10^{-2} corresponding to specimens 1#, 5#-7#, respectively. It is worth noting that the specimen 7# subjected to ageing for 2h possesses the strongest strain-amplitude dependence of Q^{-1}, even higher than that subjected to solution-ageing for 4h in Fig. 1. Moreover, compared to the specimen 4# subjected to ageing for 4h, the Q^{-1} can be markedly enhanced by ageing for a shorter time, suggesting that the ageing for 4h is overageing in essence. Even so, the Q^{-1} of specimen 4# still is quite higher than the maximum one of as-cast M2052 alloy reported in our previous work (See Supplementary Material, Fig. S1). Therefore, the optimal damping capacity of novel as-cast MnCuNiFeZnAl alloy can be achieved by ageing at 435℃ for 2h, even higher than those obtained in the conventional as-forged M2052 high-damping alloy in the literature [23,24], and meanwhile, both sand-casting and ageing possess more

evident advantages of simplicity, economy and efficiency in industry.

Fig. 3 shows metallographic micrographs of as-cast MnCuNiFeZnAl alloys subjected to different heat treatments, corresponding to specimens 1#, 5#-7# respectively. The obvious dendritical microstructures composed of dark dendrites with a few millimeters in length and several micrometers in width and light interdendritic spacings can be observed in the specimen 1#, in which the dark regions are Mn-rich dendrites and the light areas are Cu-rich spacings. This is because the coagulation of as-cast MnCuNiFeZnAl alloy is a typical mushy freeze, during which the slow cooling rate of sand-casting induces the occurrence of casting segregation and finally results in the formation of dendrite microstructures. To be specific, the Mn-rich dendrites can be precipitated primarily from liquid phase due to its relatively high melting point by Mn-enrichment and then Cu-rich spacings formed among them with the further decrease of temperature.

Compared to the microstructure of specimen 1#, the dimensions and thickness of dark Mn-rich dendrites in the specimen 5# is obviously smaller, indicating that the macrosegregation of specimen 5# is markedly weakened by homogenization-ageing of as-cast MnCuNiFeZnAl alloy. Likely, the casting segregation of specimen 6# is also weakened to a certain extent by solution-ageing, but slightly better than that of specimen 5# due to the significantly shorter holding time during solution treatment at elevated temperatures. In contrast, the dendritical microstructure feature of as-cast MnCuNiFeZnAl alloy subjected to ageing at 435℃ for 2h in the specimen 7# has no evident difference in comparison with the original as-cast one. The present

experimental results demonstrate that the dendrite segregation can be essentially reduced by homogenization treatment of as-cast alloy for a relatively long time, while the solution treatment for an evidently shorter time, even if at slightly higher temperatures, gives rise to the reduction less.

Fig. 4 shows the temperature dependence of Q^{-1} of as-cast MnCuNiFeZnAl alloys subjected to different heat treatments at a strain-amplitude of $\varepsilon=2\times10^{-4}$ and a test frequency of 1 Hz, corresponding to specimens 1#, 5#-7# respectively. It is clear that the Q^{-1} at room temperature just has a little disparity among specimens 5#-7#, much higher than the original as-cast one. However, as the temperature gradually increases, the Q^{-1} changes remarkably. The obvious decline of Q^{-1} for specimens 5#-7# occurs at 50℃, 55℃ and 70℃ respecitvely, which is normally defined as usage temperature that is one of the most critical index for engineering applications of damping alloys. In contrast, the Q^{-1} of the original as-cast MnCuNiFeZnAl alloy continually decreases with the increase of test temperature and no obvious steady stage can be found, implying that its usage temperature is just a little more than room temperature, presumably 43℃. As a result, the good damping capacity and high usage temperature can be achieved simultaneously by ageing at 435℃ for 2h of the novel as-cast MnCuNiFeZnAl alloy, which probably is a promising candidate toward engineering applications of Mn-Cu based damping alloys.

Fig. 5 shows the XRD patterns of as-cast MnCuNiFeZnAl alloys subjected to different heat treatments, corresponding to specimens 1#, 5#-7# respectively. Obviously, both γ and γ' phases can are observed in all these specimens, indicating

that the f.c.c-f.c.t phase transformations have taken place in the cooling processes of different heat treatments. Aside from the parent phase γ, the produced γ' phase by f.c.c-f.c.t phase transformation is antiferromagnetic and plays a crucial role in the damping capacity. It has been known that when the Mn-enrichment in the γ matrix is sufficient enough, the T_t can be raised to above room temperature and twinning plates of produced γ' phase tend to develop in a self-accommodation manner [25]. Typically, the c axis of γ' lattice is compressed and the a axis is elongated, resulting in the c/a ratio less than 1, which can be confirmed by the obvious splits of {220} characteristic peak shown in Fig. 5b. Moreover, it is well-recognized that the dimensions change of c and a axes of γ' lattice can be featured as lattice distortion (*a/c*-1), which can be calculated quantitatively by the Equation (1) below:

$$\frac{1}{d^2} = \frac{H^2 + K^2}{a^2} + \frac{L^2}{c^2} \quad (1)$$

where d refers to the interplanar spacing of (H K L) plane of γ' phase, a and c to the lattice parameters of γ' phase. According to the Equation (1), the a and c values for specimens 1#, 5#-7# can be estimated by the split peak positions of {220} peak in the XRD patterns, as listed in Table 2. Noticeably, the largest lattice distortion of γ' during f.c.c-f.c.t phase transformation can be obtained in the specimen 7#, which would be accountable for the optimal damping capacity, as discussed detailedly in the following part.

In contrast, the XRD pattern of as-cast MnCuNiFeZnAl alloy subjected to ageing at 435℃ for 4h, corresponding to specimens 4#, is further examined, as shown in Fig. 6. Intriguingly, the additional α-Mn phase can be identified in the specimen 4#, while

there is no obvious α-Mn phase existence in the 2h-aged specimen. Note that the precipitated α-Mn phase during overageing is paramagnetic and cannot contribute to the improvement of damping capacity [26]. This is why the damping capacity of the 2h-aged specimen can be much better than the 4h-aged one.

The relationship among lattice distortion (*a/c*-1), Q^{-1} (at a strain amplitude of $\varepsilon=2\times10^{-4}$) and usage temperature of as-cast MnCuNiFeZnAl alloys subjected to different heat treatments, corresponding to specimens 1#, 5#-7# respectively, is plotted in Fig.7. Clearly, the lattice distortion is positively related to the Q^{-1}, namely the larger the lattice distorition, the better the damping capacity. The Cochardt's magnetomechanical damping model revealed a positive association of damping capacity with saturation magnetostriction constant (λ) under the same strain amplitude [27]. The value of λ can be estimated by means of the lattice parameters (a and c) of γ' phase through Equation (2) as follows [28]:

$$\lambda=\frac{1}{4}V_f\left(\frac{a-c}{c}\right) \qquad (2)$$

where V_f denotes the total volume fraction of antiferromagnetic Mn-rich regions. Evidently, in this case, the λ is proportional to *a/c*-1 due to the negligible difference in V_f based on the XRD results in Fig. 5. Thus, the larger the lattice distorition is, the greater the λ is, and the better the damping capacity is.

It also can be found that the usage temperature has very similar change tendency with the lattice distortion and Q^{-1}, which would critically depend on the Mn content in Mn-Cu based alloys, as discussed detailedly in the following section. This present results indicate that the good damping capacity and high usage temperature can be

obtained simultaneously in the novel as-cast alloy, implying that the developed MnCuNiFeZnAl alloy system in this work probably is a new promising candidate of Mn-Cu based high-damping alloys toward engineering applications.

Fig. 8 shows the SEM micrographs of as-cast MnCuNiFeZnAl alloys without subsequent heat treatment, with homogenization at 850℃ for 24h followed by quenching into cool water and with solution treatment at 900℃ for 1h followed by quenching into cool water, respectively. The micron-sized Mn-rich dendrites and Cu-rich interdendritic spacings can be observed clearly in the original as-cast MnCuNiFeZnAl alloy, while indistinct dendrite microstructure can be discerned in the homogenized and solution-treated as-cast alloys in which the solution-treated one is slightly distinct relative to the homogenized one. Table 3 further shows the compositional EDS analysis corresponding to typical Mn-rich and Cu-rich regions pointed out in Fig. 8. It can be easy to find that the average Mn content in Mn-rich regions of as-cast MnCuNiFeZnAl alloy is 79.23 at.%, while it markedly decreases to 68.20 at.% after homogenization at 850℃ for 24h, just slightly higher than the designed Mn content (65.58 at.%) of original MnCuNiFeZnAl alloy, indicating that homogenization treatment can give rise to the obvious reduction of Mn segregation in the dendrites of as-cast MnCuNiFeZnAl alloy. In contrast, the average Mn content in Mn-rich regions of as-cast alloy decreases to 73.42 at.% after solution treatment at 900℃ for 1h, implying that, in this case, the weakening of Mn segregation in the dendrites of as-cast alloy by solution treatment is remarkably less than that by homogenization for a relatively long time although the solution temperature is slightly

higher.

It has been known that the lattice distortion of γ' phase during f.c.c-f.c.t phase transformation in Mn-Cu based alloys takes place below T_t, which is essentially dependent on the Mn content in Mn-Cu based alloys [10]. The more the Mn content is, the higher the T_t is, the larger the lattice distortion is, and thus the higher the damping capacity and usage temperature would be. As mentioned in Introduction section, when Mn-Cu based alloys are subjected to ageing in the temperature range of miscibility gap (400℃~600℃), the γ parent phase can be broken up into Mn-enrichment and Cu-enrichment at the nanoscale through spinodal decomposition due to the decrease of strain energy, characteristic of 'tweed' microstructure [12,13,29]. In this case, the maximal nanoscale Mn segregation can be achieved in Mn dendrites of as-cast MnCuNiFeZnAl alloy by spinodal decomposition upon ageing at 435℃ for 2h, over which the Mn segregation reduces markedly due to the precipitation of α-Mn. Thus, among all the specimens, the content of Mn in Mn-rich regions of specimen 7# is highest, which is directly responsible for the best damping capacity and highest usage temperature. It will be further discussed based on the calculation on Mn concentration (C_{Mn}) in nanoscale Mn-rich regions as follows.

Cowlam et al. have fitted the change of lattice parameter (c/a) of γ' phase with C_{Mn} in nanoscale Mn-rich regions of Mn-Cu based alloys [30]. For Mn-Cu based alloys of $C_{Mn} > 83.4\%$ in nanoscale Mn-rich regions after spinodal decomposition, f.c.t structured γ' phase can be formed at room temperature, and the tetragonality c/a can be expressed as [26]:

$$c/a = 2.638 - 3.317c_{Mn} + 1.618{c_{Mn}}^2 \quad (3)$$

Through bringing the calculated c/a parameters of γ' phase for four specimens in Table 2 into Eqn. (3), C_{Mn} in nanoscale Mn-rich regions after spinodal decomposition can be estimated for each specimen, as listed in detial in Table 4. In addition, the average Mn content in Mn dendrites before spinodal decomposition for each specimen can be obtained from the EDS results in Table 3 and also added in Table 4 for better comparison. Evidently, the highest C_{Mn} (85.35 at.%) in nanoscale Mn-rich regions after spinodal decomposition can be acquired in the specimen 7#, implying the best damping capacity and highest usage temperature from ageing treatment for 2h of as-cast MnCuNiFeZnAl alloy. It is worthwhile noting that the spontaneous spinodal decomposition process for a very short period still can take place during the casting solidification of original MnCuNiFeZnAl alloy due to the extremely slow cooling rate of sand-casting, which is the reason that there exists a little difference between the average Mn content in Mn dendrites and the C_{Mn} in nanoscale Mn-rich regions for the specimen 1#.

Based on our present results, it can be proposed that heat treatment process has a significant influence on the damping capacity and usage temperature of novel as-cast MnCuNiFeZnAl alloy developed in this work, and thus adjusting and controlling the heat treatment process can effectively improve the damping capacity and usage temperature. Ageing at 435℃ for 2h is most beneficial for the formation of nanoscale Mn-rich regions by spinodal decomposition and further enhances the Mn segregation level in the as-cast MnCuNiFeZnAl alloy, resulting in the increase of lattice distortion

and the raise of T_t, eventually improving the damping capacity and usage temperature markedly. On the contrary, homogenization- or solution-ageing can weaken the Mn macrosegregation in Mn dendrites to different degrees and finitely enhance the C_{Mn} in nanoscale Mn-rich regions, hence just ameliorating the damping capacity and usage temperature to some extent. This work will have important implication for design and preparation of novel high-performance Mn-Cu based damping alloys toward practical industrial applications.

4. Conclusion

In Summary, a novel cast-aged Mn-26.0Cu-2.0Ni-2.0Fe-2.0Zn-3.0Al (wt.%) alloy with good damping capacity and high usage temperature has been well designed and developed in this work. The heat treatment process has a significant influence on the damping capacity and usage temperature of the as-cast MnCuNiFeZnAl alloy. Compared to the original as-cast alloy with Q^{-1} of 3.0×10^{-2} at $\varepsilon=2\times10^{-4}$ and usage temperature of 43℃, remarkable improvements of damping capacity ($Q^{-1}=5.0\times10^{-2}$) and usage temperature (70℃) can be obtained simultaneously by ageing at 435℃ for 2h. This can be ascribed to the formation of highest nanoscale Mn segregation in Mn dendrites by spinodal decomposition during the ageing. On the contrary, carrying out the homogenization or solution treatment prior to the ageing, as well as ageing for a longer period (namely overageing) can just result in the limited improvement of damping capacity and usage temperature, which is closely related to the weakening of Mn segregation at the macro/nano-scale and even the precipitation of α-Mn.

Acknowledgements

We give thanks to financial support by the National Natural Science Foundation of China (11076109), the “HongKong Scholars Programme” Funded Project (XJ2014045, G-YZ67), the China Postdoctoral Science Foundation (2015M570784), the Scientific Research Fund of Sichuan Provincial Department of Education (16ZB0002), the Sichuan University Postdoctoral Special Fund, the Fundamental Research Funds for the Central Universities, and the Talent Introduction Program of Sichuan University (YJ201410).

References

[1] J.H. Zhang, W.Y. Peng, S.Y. Gu, H.M. Deng, S.C. Chen, Damping mechanism associated with coupling between antiferromagnetic transition and martensitic transformation, Mater. Sci. Eng. A 442 (2006) 229-232.

[2] G.E. Bacon, I.W. Dunmur, J.H. Smith, R. Street, Proc. R. Soc. Lond., Ser. A, The antiferromagnetism of manganese copper alloys, Math. Phys. Eng. Sci. 241 (1957) 223-238.

[3] J.M. Vitek, H. Warlimont, On a metastable miscibility gap in gamma-Mn-Cu alloys and the origin of their high damping capacity, Met. Sci. 10 (1976) 7-13.

[4] X.Y. Wang, W.Y. Peng, J.H. Zhang, Martensitic twins and antiferromagnetic domains in gamma-MnFe(Cu) alloy, Mater. Sci. Eng. A 438 (2006) 194-197.

[5] E.H. Wang, C.H. Guo, P.J. Zhou, C.F. Lin, X.X. Han, F.C. Jiang, Fabrication, mechanical properties and damping capacity of shape memory alloy NiTi fiber-reinforced metal-intermetallic-laminate (SMAFR-MIL) composite, Mater. Design 95 (2016) 446-454.

[6] I.S. Golovin, Anelasticity of Fe-Ga based alloys, Mater. Design 88 (2015) 577-587.

[7] C. Xu, J.H. Zhang, S.J. Liu, Y.B. Jing, Y.F. Jiao, L.J. Xu, L. Zhang, F.C. Jiang, M.L. Zhang, R.Z. Wu, Microstructure, mechanical and damping properties of Mg-Er-Gd-Zn alloy reinforced with stacking faults, Mater. Design 79 (2015) 53-59.

[8] W. Guo, H. Kato, Submicron-porous NiTi and NiTiNb shape memory alloys with high damping capacity fabricated by a new top-down process, Mater. Design 78 (2015) 74-79.

[9] X. Wang, J. Zhang, Structure of twin boundaries in Mn-based shape memory alloy: A HRTEM study and the strain energy driving force, Acta Mater. 55 (2007) 5169-5176.

[10] F.X. Yin, Y. Ohsawa, A. Sato, K. Kawahara, Decomposition behavior of the gamma(Mn) solid solution in a Mn-20Cu-8Ni-2Fe (at%) alloy studied by a magnetic measurement, Mater. Trans., JIM 40 (1999) 451-454.

[11] F.X. Yin, Y. Ohsawa, A. Sato, K. Kawahara, Temperature dependent damping behavior in a Mn-18Cu-6Ni-2Fe alloy continuously cooled in different rates from the solid solution temperature, Scripta Mater. 38 (1998) 1314-1346.

[12] F. Findik, Improvements in spinodal alloys from past to present, Mater. Design 42 (2012) 131-146.

[13] J.Z. Yan, N. Li, X. Fu, Y. Zhang, The strengthening effect of spinodal decomposition and twinning structure in MnCu-based alloy, Mater. Sci. Eng. A 618 (2014) 205-209.

[14] O. Soriano-Vargas, E.O. Avila-Davila, V.M. Lopez-Hirata, N. Cayetano-Castro, J.L. Gonzalez-Velazquez, Effect of spinodal decomposition on the mechanical behavior of Fe-Cr alloys, Mater. Sci. Eng. A 527 (2010) 2910-2914.

[15] F.X. Yin, S. Takamori, Y. Ohsawa, A. Sato, K. Kawahara, A MnCuNiFe damping alloy with superior workability and easiness for recycle, J. Jpn. I. Met. 65 (2001) 607-613.

[16] F.X. Yin, Y. Ohsawa, A. Sato, K. Kohji, Decomposition of high temperature gamma(Mn) phase during continuous cooling and resultant damping behavior in Mn74.8Cu19.2Ni4.0Fe2.0 and Mn72.4Cu20.0Ni5.6Fe2.0 alloys, Mater. Trans., JIM 39 (1998) 841-848.

[17] T. Sakaguchi, F.X. Yin, Holding temperature dependent variation of damping capacity in a MnCuNiFe damping alloy, Scripta Mater. 54 (2006) 241-246.

[18] T. Tanji, S. Moriwaki, N. Mio, T. Tomaru, T. Suzuki, T. Shintomi, Measurement of damping performance of M2052 alloy at cryogenic temperatures, J. Alloys Compd. 355 (2003) 207-210.

[19] F.X. Yin, S. Iwasaki, T. Sakaguchi, K. Nagai, Susceptibility of damping behavior to the solidification condition in the as-cast M2052 high-damping alloy, Key Eng. Mater. 319 (2006) 67-72.

[20] F.X. Yin, Y. Ohsawa, A. Sato, K. Kawahara, Characterization of the strain-amplitude and frequency dependent damping capacity in the M2052 alloy, Mater. Trans., JIM 42 (2001) 385-388.

[21] Z.Y. Zhong, W.B. Liu, N. Li, J.Z. Yan, J.W. Xie, D. Li, Y. Liu, X.C. Zhao, S.Q.

Shi, Mn segregation dependence of damping capacity of as-cast M2052 alloy, Mater. Sci. Eng. A 660 (2016) 97-101.

[22] X.X. Mou, N. Li, J.Z. Yan, Investigation of constant prestress in effecting damping capacity of Fe-15Cr-2.5Mo-1.0Ni casting ferromagnetic alloy, J. Alloys Compd. 650 (2015) 92-96.

[23] J.Z. Yan, N. Li, X. Fu, W.B. Liu, Y. Liu, X.C. Zhao, Effect of pre-deformation and subsequent aging on the damping capacity of Mn-20 at.%Cu-5 at.%Ni-2 at.%Fe alloy, Adv. Eng. Mater. 17 (2015) 1332-1337.

[24] Y. Zhang, N. Li, J.Z. Yan, J.W. Xie, Effect of the precipitated second phase during aging on the damping capacity degradation behavior of M2052 alloy, Adv. Mater. Res. 873 (2014) 36-41.

[25] A.V. Siefert, F.T. Worrell, The role of tetragonal twins in the internal friction of copper manganese alloys, J. Appl. Phys. 22 (1951) 1257-1259.

[26] F.X. Yin, Y. Ohsawa, A. Sato, K. Kawahara, X-ray diffraction characterization of the decomposition behavior of gamma(Mn) phase in a Mn-30at. % Cu alloy, Scripta Mater. 40 (1999) 993-998.

[27] A.W. Cochardt, The origin of damping in high-strength ferromagnetic alloys, J. Appl. Mech. T 20 (1953) 196-200.

[28] S. Laddha, D.C. Vanaken, On the application of magnetomechanical models to explain damping in an antiferromagnetic copper-manganese alloy, Metall. Mater. Trans. A 26 (1995) 957-964.

[29] J.H. Zhang, Typed-new multifunctional Mn-rich antiferromagnetic alloys, Curr.

Opin. Solid St. M. 9 (2005) 326-330.

[30] N. Cowlam, G.E. Bacon, L. Gillott, Changes in cell dimensions at martensitic-transformation in gamma-Mn-Cu alloys, J. Phys. F: Met. Phys. 7 (1977) L315-L319.

Figure Captions

Figure 1. Strain-amplitude dependence of Q^{-1} of as-cast MnCuNiFeZnAl alloys subjected to different heat-treatments containing ageing for 4h at a test frequency of 1 Hz.

Figure 2. Strain-amplitude dependence of Q^{-1} of as-cast MnCuNiFeZnAl alloys subjected to different heat-treatments containing ageing for 2h at a test frequency of 1 Hz.

Figure 3. Metallographic micrographs of as-cast MnCuNiFeZnAl alloys subjected to different heat treatments.

Figure 4. Temperature dependence of Q^{-1} of as-cast MnCuNiFeZnAl alloys subjected to different heat treatments. The strain-amplitude is $\varepsilon=2\times10^{-4}$ and the heating rate is 2℃/min.

Figure 5. (a) XRD patterns of as-cast MnCuNiFeZnAl alloys subjected to different heat treatments; (b) Clear splits of {220} characteristic peaks at a high-magnification.

Figure 6. XRD pattern of as-cast MnCuNiFeZnAl alloy subjected to ageing at 435℃ for 4h.

Figure 7. The relationship among lattice distortion (a/c-1), Q^{-1} (at a strain of $\varepsilon=2\times10^{-4}$) and usage temperature of as-cast MnCuNiFeZnAl alloys subjected to different heat treatments.

Figure 8. SEM micrographs of as-cast MnCuNiFeZnAl alloys (a) without subsequent treatment, (b) with homogenization at 850℃ for 24h followed by quenching into cool water, and (c) with solution treatment at 900℃ for 1h followed by quenching into

cool water.

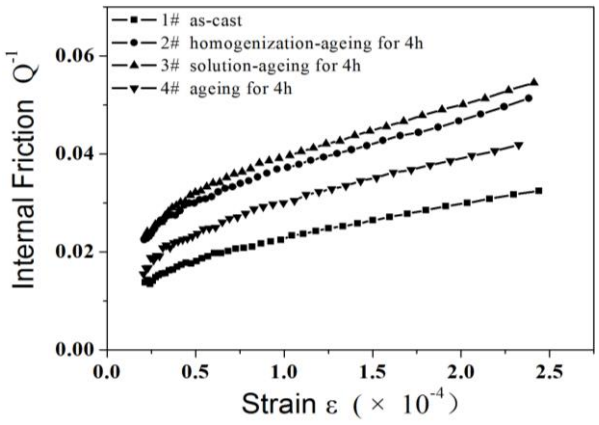

Fig. 1. Strain-amplitude dependence of Q^{-1} of as-cast MnCuNiFeZnAl alloys subjected to different heat-treatments containing ageing for 4h at a test frequency of 1 Hz.

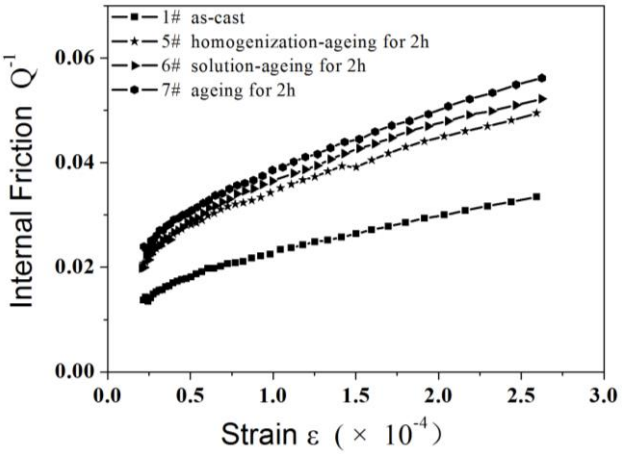

Fig. 2. Strain-amplitude dependence of Q^{-1} of as-cast MnCuNiFeZnAl alloys subjected to different heat-treatments containing ageing for 2h at a test frequency of 1 Hz.

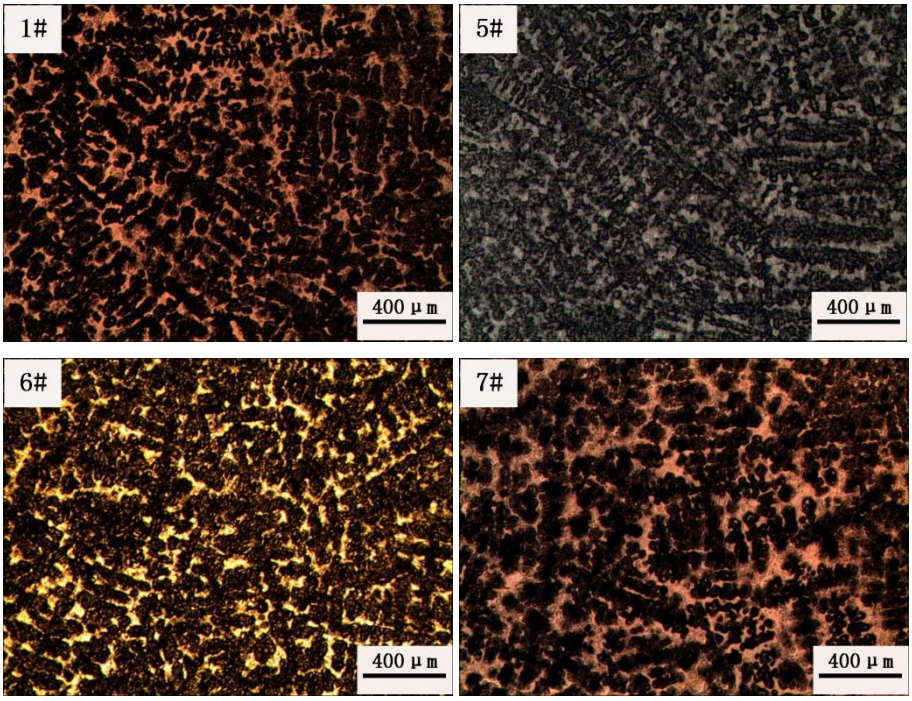

Fig. 3. Metallographic micrographs of as-cast MnCuNiFeZnAl alloys subjected to different heat treatments.

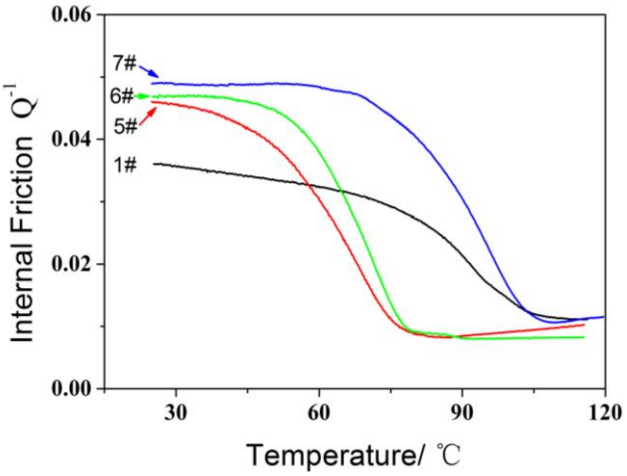

Fig. 4. Temperature dependence of Q^{-1} of as-cast MnCuNiFeZnAl alloys subjected to different heat treatments. The strain-amplitude is $\varepsilon=2\times10^{-4}$ and the heating rate is 2℃/min.

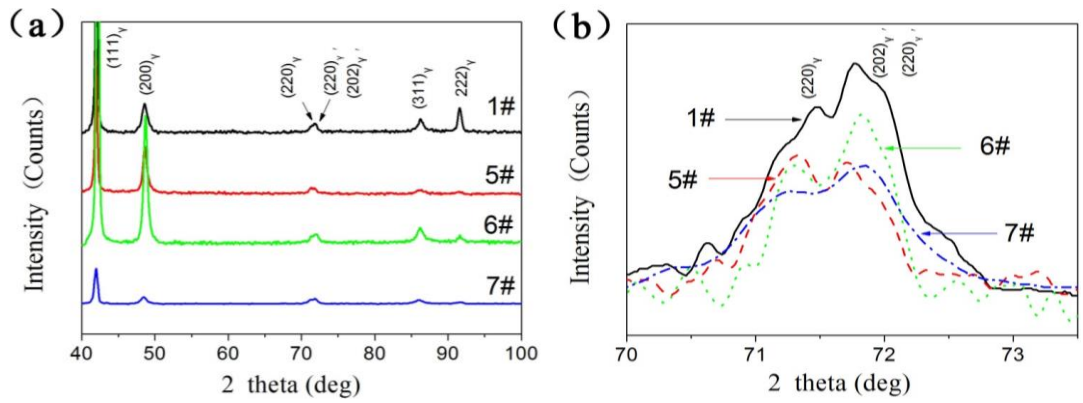

Fig. 5. (a) XRD patterns of as-cast MnCuNiFeZnAl alloys subjected to different heat treatments; (b) Clear splits of {220} characteristic peaks at a high-magnification.

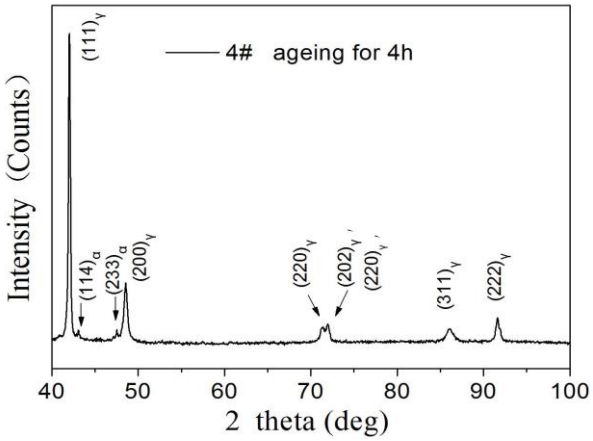

Fig. 6. XRD pattern of as-cast MnCuNiFeZnAl alloy subjected to ageing at 435℃ for 4h.

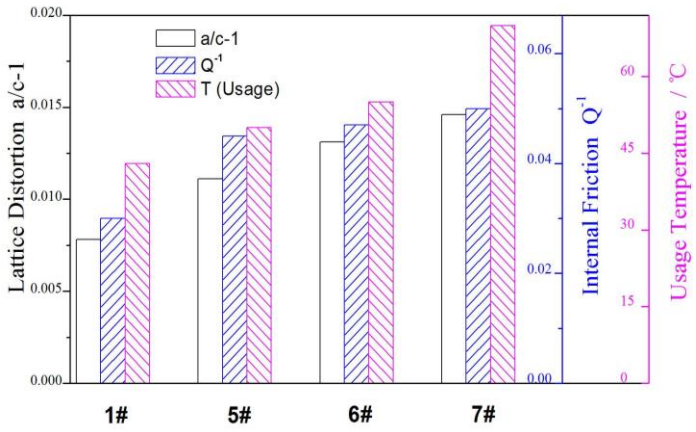

Fig. 7. The relationship among lattice distortion (*a*/*c*-1), Q^{-1} (at a strain of $\varepsilon=2\times10^{-4}$) and usage temperature of as-cast MnCuNiFeZnAl alloys subjected to different heat treatments.

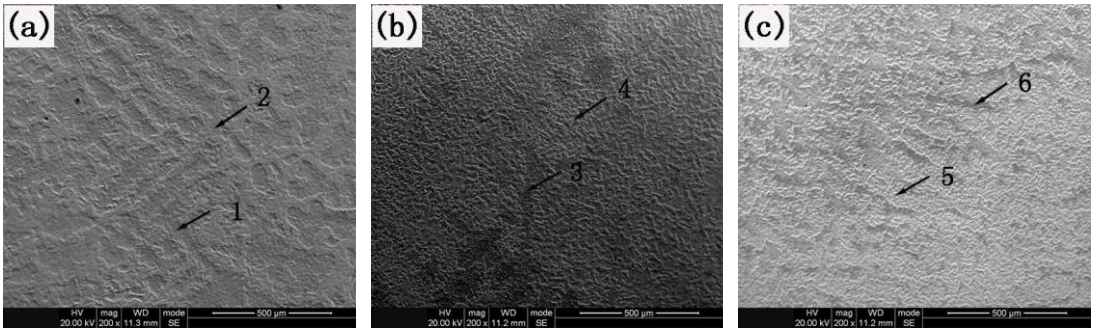

Fig. 8. SEM micrographs of as-cast MnCuNiFeZnAl alloys (a) without subsequent treatment, (b) with homogenization at 850℃ for 24h followed by quenching into cool water, and (c) with solution treatment at 900℃ for 1h followed by quenching into cool water.

Table 1. Detailed heat treatment conditions of seven types of specimens.

Specimens	Heat treatment conditions
1#	Original as-cast alloy without subsequent heat treatment (as-cast)
2#	Homogenizing at 850℃ for 24h, and then quenching into cool water before ageing at 435℃ for 4h (homogenization-ageing for 4h)
3#	Solution treatment at 900℃ for 1h, and then quenching into cool water before ageing at 435℃ for 4h (solution-ageing for 4h)
4#	Ageing at 435℃ for 4h (ageing for 4h)
5#	Homogenizing at 850℃ for 24h, and then quenching into cool water before ageing at 435℃ for 2h (homogenization-ageing for 2h)
6#	Solution treatment at 900℃ for 1h, and then quenching into cool water before ageing at 435℃ for 2h (solution-ageing for 2h)
7#	Ageing at 435℃ for 2h (ageing for 2h)

Table 2. Calculated lattice parameters and lattice distortion of as-cast MnCuNiFeZnAl alloys subjected to different heat-treatments by Equation (1).

Specimens	Lattice Parameter [Å]				
	Indexed Interplanar spacing		Calculated lattice parameter		Lattice Distortion
	d_{220}	$d_{022\&202}$	a	c	$a/c-1$
1#	1.3190	1.3139	3.7307	3.7020	0.0078
5#	1.3215	1.3142	3.7378	3.6968	0.0111
6#	1.3219	1.3133	3.7389	3.6907	0.0131
7#	1.3223	1.3127	3.7400	3.6863	0.0146

Table 3. Compositional EDS analysis corresponding to typical Mn-rich and Cu-rich regions in Fig. 8.

	Region	Site	Mn (at.%)	Cu (at.%)	Ni (at.%)	Fe (at.%)	Zn (at.%)	Al (at.%)
Fig. 8a	Mn-enrichment	1	79.23	9.83	1.80	1.89	1.60	5.65
	Cu-enrichment	2	53.98	35.86	1.89	1.98	0.23	6.05
Fig. 8b	Mn-enrichment	3	68.20	20.06	1.98	2.02	1.92	5.82
	Cu-enrichment	4	62.12	27.77	1.87	2.00	0.25	5.99
Fig. 8c	Mn-enrichment	5	73.42	15.03	2.01	1.94	1.86	5.74
	Cu-enrichment	6	58.87	31.43	1.87	1.93	0.31	5.59

Table 4. Comparison between average Mn content in Mn dendrites before spinodal decomposition and C_{Mn} in nanoscale Mn-rich regions after spinodal decomposition (at.%).

Specimens	1#	5#	6#	7#
Average Mn content in Mn dendrites before spinodal decomposition	79.23	68.20	73.42	79.23
C_{Mn} in nanoscale Mn-rich regions after spinodal decomposition	84.18	84.75	85.08	85.35